Composition and Cr- and Fe-speciation of dust generated during ferrochrome production in a DC arc furnace

Berryman, Eleanor J.; Paktunc, Dogan; Kingston, David; Beukes, Johan P.

Publisher's version / Version de l'éditeur:
https://doi.org/10.1016/j.clet.2021.100386
Cleaner Engineering and Technology, 6, C, 2022-01-08

Cleaner Engineering and Technology 6 (2022) 100386

Contents lists available at ScienceDirect

Cleaner Engineering and Technology

journal homepage: www.sciencedirect.com/journal/cleaner-engineering-and-technology

Composition and Cr- and Fe-speciation of dust generated during ferrochrome production in a DC arc furnace

Eleanor J. Berryman [a], Dogan Paktunc [a,*], David Kingston [b], Johan P. Beukes [c]

[a] CanmetMINING, Natural Resources Canada, 555 Booth Street, Ottawa, ON, K1A 0G1, Canada
[b] National Research Council Canada, 1200 Montreal Rd, Ottawa, ON, K1A 0R6, Canada
[c] Chemical Resource Beneficiation, North-West University, Potchefstroom, 2520, South Africa

ARTICLE INFO

Keywords:
Hexavalent chromium
Cr(VI)
Chromite
Ferrochrome
Smelting
DC furnace

ABSTRACT

A potential hazard associated with ferrochrome production is the unintentional generation of Cr(VI) in the off-gas dusts produced during smelting. Cr(VI) is a well-known environmental toxin and genotoxic carcinogen. Although Cr(VI) has been identified in baghouse dusts associated with submerged-arc furnaces, its occurrence in DC-arc-furnace dusts has not been previously investigated. In this study, we report the bulk composition and phase make-up, as well as the surface and bulk speciation of Cr and Fe of dusts generated during smelting of chromite ore under basic slag conditions in a pilot-scale DC arc smelter. Dusts are captured from both within the DC furnace as well as along the off-gas handling stream, after passing through the afterburner. The dusts primarily comprise feed material (chromite, flux, reductant), aerosolized slag, and glassy spherules, interpreted as off-gas condensates. Dusts collected from within the furnace, known as freeboard dusts, are dominated by feed materials, with elevated amounts of flux (lime) and lesser amounts of slag and spherules. In contrast, spherules dominate dusts collected along the off-gas handling stream by dust separators that capture the increasingly fine-grained fraction of dust, with the highest proportion of spherules occurring in baghouse dusts. Chromite is the primary host of Cr in all dust samples, whereas the spherules have low Cr contents. Cr(VI) was identified by X-ray photoelectron spectroscopy in the surfaces of dust collected from all parts of the smelter system considered, including from the furnace freeboard, despite the overall reducing conditions present therein. Cr(VI) concentrations are sufficiently high in dusts collected from the off-gas handling stream (post-afterburner, cyclone, and baghouse) to be detected in the bulk dust samples by X-ray absorption spectroscopy. The higher concentration of Cr(VI) in the finer-grained off-gas dusts, especially the baghouse dusts, is consistent with the increased abundance of spherules, the major Cr(VI)-hosting phase, in these samples. Fe is similarly more oxidized in dusts collected down the off-gas handling stream compared to dusts collected from within the furnace, which are dominated by Fe(II). Fe(III) hosted by FeOOH is predominate in dusts collected from all locations along the off-gas handling stream. These results demonstrate that there is sufficient oxygen ingress and sufficiently high temperatures in the closed DC furnace for Cr(VI) to be generated in the freeboard off-gas dusts. Cr(VI) is associated with the finest grained fraction of dusts, underlining the importance of ensuring the continual improvement of dust-capture systems, especially in terms of their ability to target increasingly finer fractions of dust.

1. Introduction

Ferrochrome (FeCr) is an alloy primarily used in stainless-steel production, owing to the corrosion-resistant properties that chromium imparts to the steel. Ferrochrome is commonly produced by the carbothermic reduction of chromite, a spinel-group mineral with end-member formula $FeCr_2O_4$, which is better represented with the general formula $(Mg,Fe^{2+})(Cr,Fe^{3+},Al)_2O_4$ (Irvine 1965; Haggerty 1991) because of common substitution of Fe by Mg and Cr by Al and Fe^{3+}.

Although Cr(III), the oxidation state of Cr in chromite, is the most common naturally occurring oxidation state of Cr, Cr(VI) is also stable and environmentally significant (Bartlett and James 1988; Oze et al.,

Abbreviations: FeCr, Ferrochrome; SAF, Submerged Arc Furnace; µXANES, micro-X-ray Absorption Near Edge Structure; XANES, X-ray Absorption Near Edge Structure; XRD, X-ray Diffraction; XRF, X-ray Fluorescence; XAS, X-ray Absorption Spectroscopy; XPS, X-ray Photoelectron Spectroscopy; DSC, Dry Solid Charge.

* Corresponding author.
E-mail addresses: eleanor.berryman@nrcan-rncan.gc.ca (E.J. Berryman), dogan.paktunc@canada.ca (D. Paktunc).

https://doi.org/10.1016/j.clet.2021.100386
Received 20 August 2021; Received in revised form 23 November 2021; Accepted 28 December 2021
Available online 30 December 2021

2007). Whereas Cr(III)-bearing compounds are largely insoluble and therefore have low environmental mobility and toxicity, Cr(VI)-bearing compounds like chromates tend to have higher solubility and are well-known environmental toxins as well as being genotoxic carcinogens (Arita and Costa 2011). Naturally occurring Cr(VI) is known to form in the presence of oxidants, such as manganese oxides or peroxide (Oze et al., 2007). However, most significant occurrences of Cr(VI) are linked to anthropogenic sources, especially chromate manufacturing, and to a lesser extent, leather tanning, electroplating, and FeCr production (Bartlett and James 1988; Beukes et al., 2017).

There are a number of process options used for the carbothermic reduction of chromite to produce FeCr. The most common are: i) open/semi-open submerged-arc furnace (SAF) smelting of chromite ore and/or pelletized/briquetted chromite composites; ii) closed SAF smelting of oxidative sintered chromite pellets; iii) closed SAF smelting of pre-reduced chromite composite pellets; and iv) direct-current (DC) furnace smelting of fine chromite ore (Beukes et al., 2017). The main chemical reaction in all cases is the reduction of Cr(III) in chromite to Cr (0) in ferrochrome. Despite being designed for Cr reduction, noteworthy concentrations of Cr(VI) (~mg/kg) have been identified in dusts captured by: i) the baghouse filters commonly associated with open/semi-open SAFs (Cox et al., 1985; Maine et al., 2005; Du Preez et al., 2017); and ii) in the sludges and circulating water from the wet gas scrubbers (Gericke 1995) commonly associated with closed SAFs smelting oxidative and pre-reduced chromite composite pellets (Beukes et al., 2017). The presence of leachable Cr(VI) concentrations in fine ferrochrome-smelter dusts that are exceeding the regulation limits in South Africa was reported by Ma and Gerbers-Craig (2006).

To the best of our knowledge, the present study is the first systematic investigation of the net abundance of Cr(VI) in ferrochrome-smelter dusts originating from DC furnaces. The insight gained from this study is timely, considering the increasing abundance and production capacity of this technology for FeCr smelting (with furnaces up to 72 MW now in operation) (Jones 2014). The inclusion of dusts captured from within the furnace freeboard, as well as along the off-gas stream, is particularly novel, because it allows the unaltered dusts to be studied directly. Previous studies have focused on baghouse dusts collected from open/semi-open SAFs and have relied on wet-chemical techniques to determine bulk Cr(VI) contents (Cox et al., 1985; Gericke 1995; Maine et al., 2005; Du Preez et al., 2017). These techniques can be affected by inter-conversion of Cr(III) and Cr(VI) and they do not provide direct information on the speciation of chromium (Ashley et al., 2003). The use of synchrotron-based X-ray absorption spectroscopy (XAS) and X-ray photoelectron spectroscopy (XPS) in the present study allows for the identification of Cr(VI) in the bulk dusts (XAS) and particle surfaces (XPS) with minimal sample handling. This minimizes the possibility of reducing or oxidizing reactions taking place during sample preparation and analysis. In addition, these spectroscopic techniques have the additional advantage of providing information on the speciation of Fe as well as Cr.

The results presented here indicate variations in the phase make-up, bulk composition, Cr and Fe speciation of different fractions of dusts collected from the smelter. The resulting insight into the Cr(VI)-bearing fractions of the dust and their abundance within different parts of the smelter system can be applied to optimizing dust-capture systems, ensuring that fugitive Cr(VI)-bearing dusts resulting from DC-furnace ferrochrome smelting are minimized. In addition, the knowledge gained on process conditions promoting the formation of Cr(VI) is helpful in developing measures to minimize or prevent the formation of Cr(VI) during smelting.

2. Methods

2.1. Pilot-scale smelter tests and dust collection

Smelter dusts were generated in a 300-kW pilot-scale DC arc furnace at the facilities of Expert Processing Solutions in Sudbury, Ontario, Canada. Chromite ore samples from the Black Thor deposit, one of Canada's Ring of Fire deposits in northern Ontario, were smelted under basic [$(CaO + MgO)/SiO_2 = 1.3$–1.4] slag conditions in seven smelting tests. The smelting conditions for each test are provided in Table 1, with the feed compositions provided in SI Table 1. Individual tests varied in terms of the ore size fraction used [whole ore (<4.75 mm), fine fraction (<1.68 mm) and coarse fraction (1.68–4.75 mm)], the average feed-rate (31–59 kg ore/hr), the proportion of flux in the feed (0.146–0.200 kg limestone/kg ore and 0.092–0.120 kg silica/kg ore), and the test duration (~2.5–10.5 h). Although the average power during smelting (103–126 kW; Table 1) also varied, the target smelting temperature was consistently 1700°C, which is above the liquidus temperature of the targeted slag composition. A schematic of the 300-kW pilot-scale DC arc furnace and the off-gas handling system is shown in Fig. 1 and a photograph is available in Berryman et al. (2020). Fig. 2 shows the variation in the power and feed rate during each of the smelting tests, as well as the composition of the off-gas measured in the furnace (freeboard) and after the afterburner in three of the tests.

Dust samples were captured using filters placed in the gas samplers from the furnace freeboard and after the afterburner (post-afterburner) in tests 6–8 (Fig. 1). In all tests, dusts were also collected from the standard dust separators, the cyclone and baghouse. The freeboard and cyclone samples were collected during smelting, as indicated in Fig. 2. All other samples were collected at the end of each test. The dropout box samples were collected at the end of the smelting campaigns.

2.2. X-ray fluorescence (XRF) and total carbon analysis

Subsamples of collected dust were analyzed for their bulk compositions at Activation Laboratories (Ancaster, Ontario). The samples were dried at 105°C prior to loss on ignition (LOI) measurement and fusion. LOI was determined by weight loss after 2 h of sample roasting at 1050°C. The roasted sample is mixed with a fluxing mixture (lithium metaborate, lithium tetraborate and lithium bromide) and fused in platinum crucibles before XRF analysis on a Panalytical Axios Advanced wavelength dispersive XRF. Detection limits are 0.01 wt% for all measured elements.

The total carbon (C) content of the dust samples was determined by catalytic combustion that converts C in the sample to CO_2, which is subsequently detected by infrared (IR) analysis using an ELTRA instrument. The reported detection limit is 0.01 wt%.

2.3. X-ray diffraction (XRD)

The dust samples were generally fine enough to not require grinding before powder XRD analyses. The samples were placed on a zero-background plate and disseminated using a drop of acetone. Powder XRD patterns were collected using a Rigaku D/MAX 2500 rotating-anode powder diffractometer with monochromatic CuKα radiation at 40 kV, 200 mA, a step-scan of 0.02°, and a scan rate at 1°/min in 2θ from 5 to 70°. Phase identifications were made using JADE v.9.3 coupled with the ICSD and ICDD databases.

2.4. X-ray photoelectron spectroscopy (XPS)

XPS was done in the Cr 2p (569–599 eV) and Fe 2p (700–740 eV) binding-energy ranges on subsamples of the ferrochrome smelter dusts using a Kratos Axis Ultra XPS equipped with a monochromatic Al X-ray source at the National Research Council of Canada. Following a 160-eV survey scan to identify the location of the major spectral features, three high-resolution spectra were collected for each element per sample under an 8.0×10^{-9}-torr chamber pressure using a 14-kV accelerating voltage, a 10-mA current, and a 300 × 700-μm aperture. Charge build-up was compensated for using the Axis charge balancing system. The high-resolution spectra were recorded in 30 sweeps at a 20-eV pass

Table 1
Summary of smelting-test operating conditions.

Test no.	Ore size fraction (mm)	Average ore feed-rate (kg/hr)	Average DSC feed-rate (kg/hr)	Limestone/Ore by mass	Silica/Ore by mass	Average power (kW)	Duration (h: min)
1	<4.75	34	51	0.190	0.100	111	10:21
2	<1.68	40	62	0.200	0.120	121	02:35
3	1.68–4.75	36	56	0.200	0.120	103	02:46
5	<4.75	35	52	0.146	0.092	104	03:23
6	<4.75	42	46	0.190	0.100	118	09:00
7	<4.75	59	54	0.190	0.100	126	10:04
8	<4.75	31	29	0.190	0.100	121	07:03

Note: DSC stands for Dry Solid Charge.

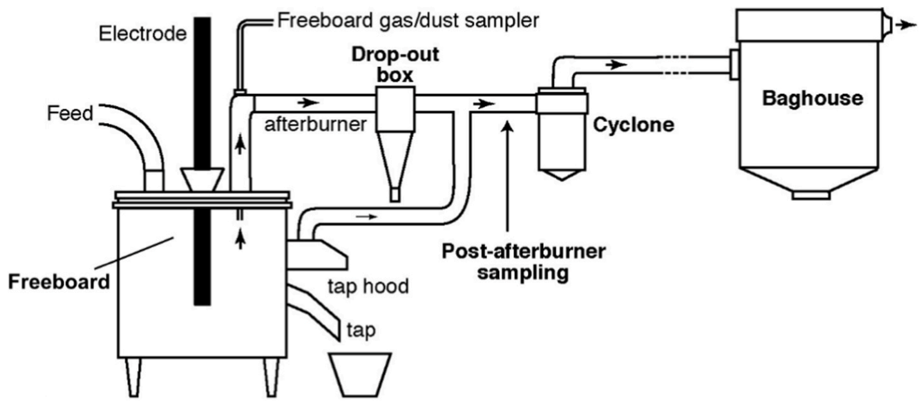

Fig. 1. A schematic of the 300-kW pilot-scale DC arc furnace and the off-gas handling system used to generate and capture smelter dusts produced during ferrochrome smelting. Locations indicated by bold text (i.e., freeboard, dropout box, post-afterburner, cyclone, and baghouse) indicate dust sampling locations. The arrows indicate the direction of off-gas movement through the smelter system.

energy with a 100-meV step size and a 239-ms dwell time per step, for a 36-min total analysis time per element.

Peak fitting of the spectra was done using the CasaXPS (ver. 2.3.19PR1.0) data-processing software. Following Shirley background-correction procedures, curve fitting was done using primarily Gaussian-Lorentzian functions, with the exception of select cases where a Lorentzian Asymmetric line shape was preferred. The high-resolution spectra were calibrated to an adventitious C 1s signal at 284.8 eV. The reference spectra used for peak fitting were taken from Grosvenor et al. (2004) and Biesinger et al. (2004, 2011) and quantification of species abundances used sensitivity factors provided by CasaXPS' Scofield element library.

2.5. X-ray absorption spectroscopy (XAS)

X-ray absorption near-edge structure (XANES) spectra were recorded for all samples and reference standards around the Cr and Fe K-edges at beamline 6-BM of NSLS-II. The dusts and reference standards were prepared as fine powders (ground with an agate mortar and pestle, when necessary) and mounted using the standard tape method (Calvin 2013). Packets of the mounted samples were layered to achieve ~1 absorption length around the Cr K-edge. A silicon (111) monochromator was used. XANES spectra (four repetitions for Cr and three for Fe) were recorded at room temperature in transmission mode using an unfocussed beam (8 × 1.2 mm). Energy ranges were 5789–6533 eV for the Cr K-edge with a step size of 0.2 eV over the pre-edge and edge regions, and 6912–7656 eV for the Fe K-edge with a step size of 0.5 eV over the edge region. Energy calibrations were done using Cr and Fe metal foils. Data reduction and linear combination fitting analyses (LCA) were done using the Demeter software package (Ravel and Newville 2005).

3. Results

3.1. Bulk major-element composition

All the DC-furnace smelter dusts (freeboard, cyclone, baghouse and dropout box) are dominated by SiO_2 and MgO, with lesser amounts of Cr_2O_3, Fe_2O_3, CaO, and Al_2O_3 (Table 2). The freeboard dusts and some of the cyclone dust samples are distinguished by their high CaO contents (Fig. 3). Compositions of the individual bulk samples are given in SI Table 2.

Fig. 4 shows the dust compositions based on sampling location relative to their associated smelter-feed composition. In general, dusts collected from the baghouse and the cyclone are enriched in MgO and SiO_2 relative to the feed, on average by ~19 and 13 wt%, respectively. They are also slightly enriched in CaO, on average by ~3 wt%, with the cyclone dusts showing higher CaO values than the baghouse dusts. In contrast, the baghouse and cyclone dusts are depleted in Cr_2O_3 relative to the feed, on average by 13 wt%, and to a lesser extent in Fe_2O_3 (total Fe) and Al_2O_3, on average by 3 and 1 wt%, respectively. Dusts collected from the freeboard show similar, albeit less pronounced, compositional differences from the feed as the cyclone and baghouse dusts, with the exception of CaO. For instance, the freeboard dusts are also enriched in MgO and SiO_2, but to a lesser extent than the cyclone and baghouse dusts, on average by 9 wt% for both components. They are also slightly depleted in Cr_2O_3 by 5 wt%, in Fe_2O_3 (total Fe) by 5 wt%, and in Al_2O_3 by 2 wt% relative to the feed. The freeboard dusts are distinguished from the other dusts by their greater enrichment in CaO, which is on average 16 wt% greater than the CaO content of the feed. The compositions of dusts from different sampling locations were broadly consistent across all test conditions, as shown in SI Figs. 1 and 2.

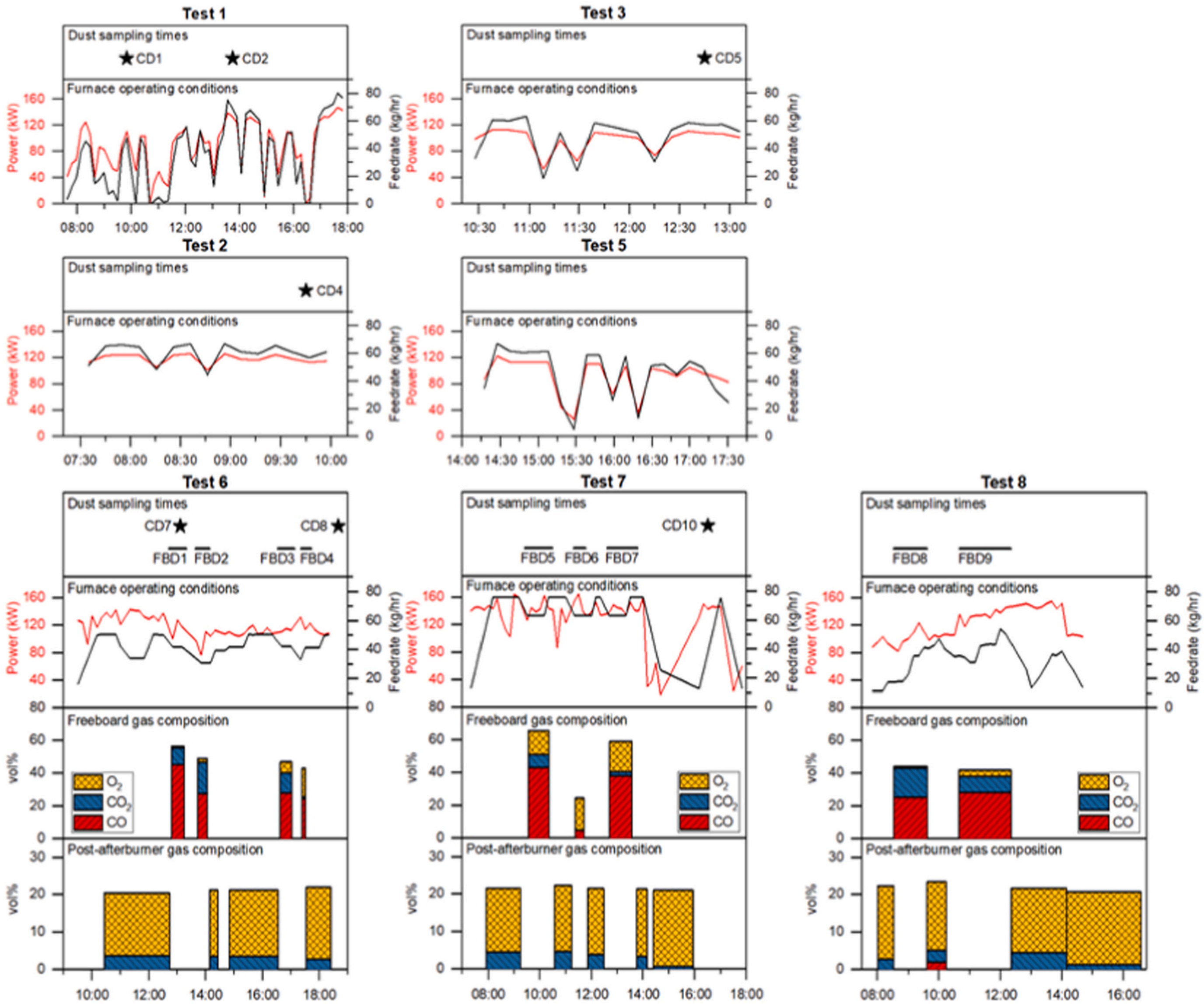

Fig. 2. Dust sampling times (indicated by star and lines) and furnace operating conditions (power and feed rate) for all smelter tests. Gas compositions measured in the furnace (freeboard) and down the off-gas stream (post-afterburner) for tests 6–8 are also shown. In the top panel of each test, star symbols indicate when the cyclone was emptied to collect cyclone dust; lines indicate the duration over which freeboard dust was collected on a filter placed within the freeboard gas sampler. All dust samples associated with each of these tests but not indicated in the respective figure were collected at the end of the test.

Table 2
Ranges of the major-element bulk composition (wt%) of smelter dusts by XRF.

	n	Cr_2O_3	Fe_2O_3	Al_2O_3	SiO_2	MgO	CaO	K_2O
Freeboard	6	13.65–17.91	7.28–10.33	6.69–7.63	7.97–27.54	13.32–27.59	18.47–31.40	0.37–2.67
Cyclone	12	4.78–30.98	2.75–13.28	4.45–20.42	10.59–35.32	21.22–35.39	4.86–29.58	0.23–1.47
Baghouse	19	3.60–27.34	2.76–21.85	2.57–12.93	16.88–36.28	10.18–46.99	2.47–9.84	0.54–4.90
Dropout box	2	17.86–22.47	10.68–13.41	8.60–8.78	9.52–18.30	17.07–24.88	14.65–25.37	0.57–0.58

Note: n: number of samples analyzed; Fe_2O_3 represents total iron. A complete list of the analytical results is given in SI Table 2.

3.2. Mineralogical composition (powder XRD)

The crystalline phases in the dust samples from the first pilot testing campaign identified by powder XRD are chromite, forsterite, periclase, lime, chlorite, maghemite, lizardite, halite and quartz (SI Table 3). Among these, chromite, forsterite and periclase are the dominant crystalline phases present in almost all the dust samples. Cyclone samples typically have chromite, forsterite, periclase, and lime as crystalline phases. In addition to the crystalline phases, all the samples contain amorphous material in variable quantities. Dust samples from the second pilot smelting campaign were not analyzed by XRD due to limited sample sizes. Two XRD patterns are shown as examples in SI Fig. 3.

3.3. Cr and Fe speciation on particle surfaces

The Cr and Fe surface species identified in the XPS spectra and their relative abundances are summarized in Table 3 and Figs. 5 and 6.

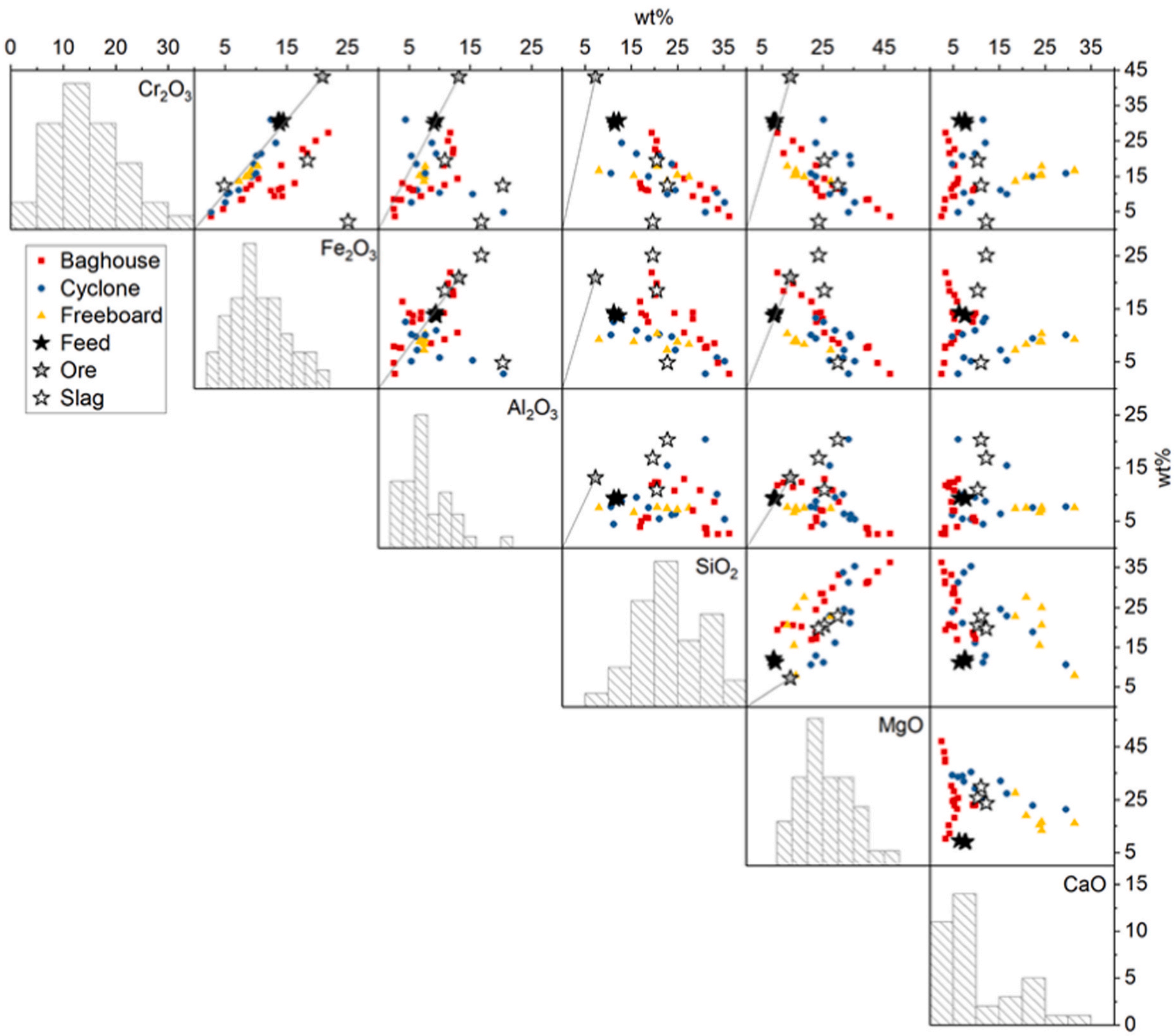

Fig. 3. Major-element bulk composition of dust samples collected from the baghouse, the cyclone, and the furnace freeboard during all smelter tests. The feed, ore, and slag compositions are indicated for comparison. Straight lines indicate compositions corresponding to varying proportions of ore content.

3.3.1. *Cr surface speciation*

The major Cr species identified on the dust surfaces were $Cr(OH)_3$ (one peak near 577.2 eV), Cr(VI) (579.6 eV), and Cr_2O_3 (five peaks near 575.6, 576.6, 577.4, 578.4 and 579.2 eV), with occasional identification of minor amounts of Cr(0) (574.3 eV) (SI Fig. 4). Cr(VI) species include various chromate species around 579.6 ± 1.5 eV including K_2CrO_4, Na_2CrO_4 and $CaCrO_4$ with binding energies of 578.4, 578.6 and 577.7 eV. Although the abundance of each species varied significantly between individual samples, on average, most surface Cr occurs as Cr_2O_3, followed closely by $Cr(OH)_3$ (Table 3; SI Table 4; Fig. 5). The only exception is dust collected on filters placed just after the after-burner (post-afterburner dust), in which $Cr(OH)_3$ was predominant in all samples. Significant amounts of Cr(VI) were identified on the surface of dusts collected from all locations in the smelter system (Table 3). The average amount of Cr(VI) was broadly consistent across sampling locations (Fig. 5). Notably, the sample with the maximum amount of surficial Cr (VI) was collected from the furnace freeboard (FBD3 from Test 6, with 40 at% of surficial Cr occurring as Cr(VI); Fig. 5 or 55 at% Cr(VI) in SI Table 4).

3.3.2. *Fe surface speciation*

The major Fe species identified on the dust surfaces were FeO (four peaks near 708.4, 709.7, 710.9, and 712.1 eV), FeOOH (five peaks near 710.3, 711.3, 712.2, 713.3, and 714.4 eV), Fe_2O_3 (five peaks near 709.9, 710.9, 711.9, 713.1, and 714.2 eV), and Fe(0) (706.9 eV) (SI Fig. 4). FeO was consistently the predominant surficial Fe species in the freeboard dusts, followed by FeOOH and Fe_2O_3. In contrast, surficial Fe in samples collected along the off-gas handling stream (i.e., the post-afterburner, cyclone, and baghouse) was predominantly FeOOH, with lesser amounts occurring as FeO. Significant amounts of Fe_2O_3 were identified mostly in the baghouse dust samples (Tables 3 and SI Table 4). The speciation of surficial Fe was broadly consistent across test conditions, showing no discernible systematic variations as a function of feed-rate or ore-size fraction in the feed.

3.4. *Bulk speciation of Cr and Fe by XANES*

The XANES spectra from around the Cr and Fe K-edges provide information on the average bulk speciation of Cr and Fe in each of the ferrochrome-smelter dust samples. Fig. 7 shows the normalized XANES spectra near the Cr and Fe K-edge regions for the dust samples and the reference standards. The Si(111) monochromator displayed a glitch in the range of 5989.3–5992.5 eV due to a crystallographic plane other than (111) in one of the Si crystals satisfying the Bragg diffraction condition. As a result, the incident photon intensity reaching the sample consistently dipped over this energy range (SI Fig. 5). This dip in monochromator intensity combined with slight inhomogeneity in certain samples created a sinusoidal glitch in the Cr K-edge spectra for the following samples: freeboard dusts FBD2, FBD3, FBD4 (Test 6); FBD5, FBD6 (Test 7); post-afterburner dusts from Tests 6 and 7; and

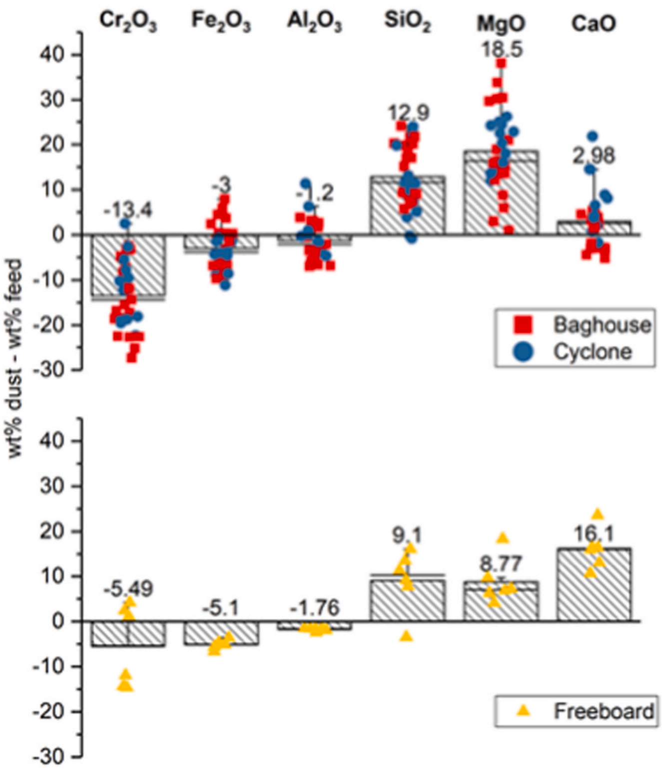

Fig. 4. Major-element bulk composition of dust samples collected from the baghouse, the cyclone, and the furnace freeboard relative to the feed composition from each respective smelter test. Data points represent individual samples; columns indicate average values; and bars median values. Data for individual tests is provided in the Supplementary Information.

possibly the baghouse dusts. In these spectra, data points in the range of the glitch (5989.3–5992.5 eV) were excluded from the spectra shown in Fig. 7, except for the baghouse dust spectra. It is important to note that the presence of this glitch did not affect the detection of the pre-edge feature at 5993.2 eV. Examples of the spectra before and after deglitching are provided in SI Fig. 5.

3.4.1. *Cr speciation*

The overall near-edge structure of all collected Cr K-edge XANES spectra matches that of the chromite standard (Fig. 7). A dashed line in Fig. 7 indicates the consistent position of the white line in the spectra of the dust samples and in the chromite standard. In some of the spectra, specifically those for dusts collected from locations along the off-gas handling stream (the post-afterburner, cyclone, and baghouse), a pre-edge feature not attributable to chromite is present at 5993.2 eV, as highlighted in Fig. 7.

Pre-edge peaks at energies below the Cr K-edge are attributed to the transition of a Cr core electron to an unoccupied antibonding tetrahedral orbital in a CrO_4^{2-} crystal field (Bianconi et al., 1991). The energies at which such pre-edge features occur depends on the energy level of the associated tetrahedral valence orbitals (Bianconi et al., 1991), with higher energy positions correlating to higher Cr valence states (Arcon et al., 1998) and the gain in intensities attributable to low-symmetry of the absorber's local environment. This correlation is apparent when comparing the position of the pre-edge feature in the spectra of chromite and Cr_2O_3 [Cr(III)] against that in the chromate standards like Na_2CrO_4, $MgCrO_4$, K_2CrO_4, and $CaCrO_4$ [Cr(VI)] (Fig. 7). The subtle pre-edge feature in the spectra of the Cr(III)-bearing species occurs at ~5991 eV contrasts to the prevalent pre-edge feature of chromates at 5993.2 eV (Fig. 7). Pre-edge peaks attributable to both oxidation states, Cr(III) and Cr(VI), are identifiable in the XANES spectra of the ferrochrome-smelter dust samples from post-afterburner, cyclone and baghouse. Linear combination fitting analysis involving all combinations of chromite, Cr_2O_3, Na_2CrO_4, $MgCrO_4$, K_2CrO_4, and $CaCrO_4$ failed to produce reasonable fits to the XANES spectra suggesting that none of the chromate standards is representative of the Cr(VI) species present in the dust.

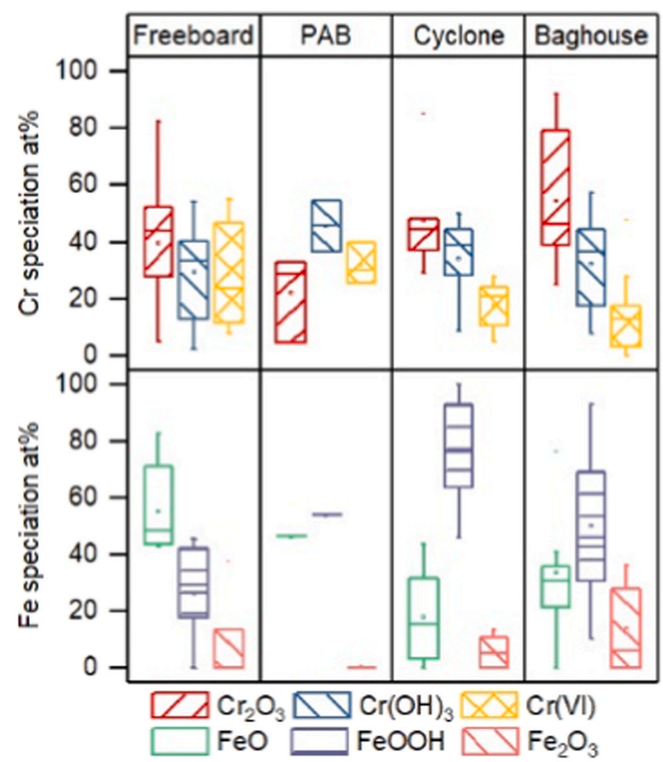

Fig. 5. Surface speciation of Cr and Fe determined by XPS. Box-and-whisker plots show the range and quartile values, with the mean indicated by a dot. Panels are organized based on dust sampling location (furnace freeboard, post-afterburner, cyclone, and baghouse), with the upper panels showing Cr surface speciation and the lower panels showing Fe surface speciation.

Table 3
Summary of Cr and Fe species on particle surfaces (at%) based on XPS.

Location	N	Cr(0)	Cr_2O_3	$Cr(OH)_3$	Cr(VI)	Fe(0)	FeO	Fe_2O_3	FeOOH
Pilot testing 1									
Cyclone	6	0.2–1.3	37.0–85.0	8.7–44.6	5.1–27.6		6.1–26.3	9.7–13.3	64.0–100.0
Baghouse	13	0.2–0.7	24.8–92.1	7.7–57.2	0.1–19.1		7.3–41.0	0.2–36.3	30.4–92.7
Dropout box	1	0.63	84.61	11.95	2.81		23.49	19.43	57.09
Pilot testing 2									
Freeboard	9	0.6–4.2	5.3–82.5	2.3–54.2	8.0–54.9	14.1–22.0	42.5–82.4	12.1–37.5	17.6–45.4
Cyclone	6	0.5–1.0	29.2–48.5	27.8–50.1	10.7–25.6		10.2–43.8	0.0–10.4	45.9–89.8
Baghouse	6	0.5–1.5	25.1–49.0	22.1–42.1	13.7–48.1	0.0–20.6	44.7–78.8		10.0–55.3
PAB	3	0.6–1.1	4.6–32.7	36.6–54.8	25.3–39.6		0.0–46.4		0.0–53.6

N: number of samples analyzed; PAB: post after-burner; Individual analyses are given in SI Table 4.

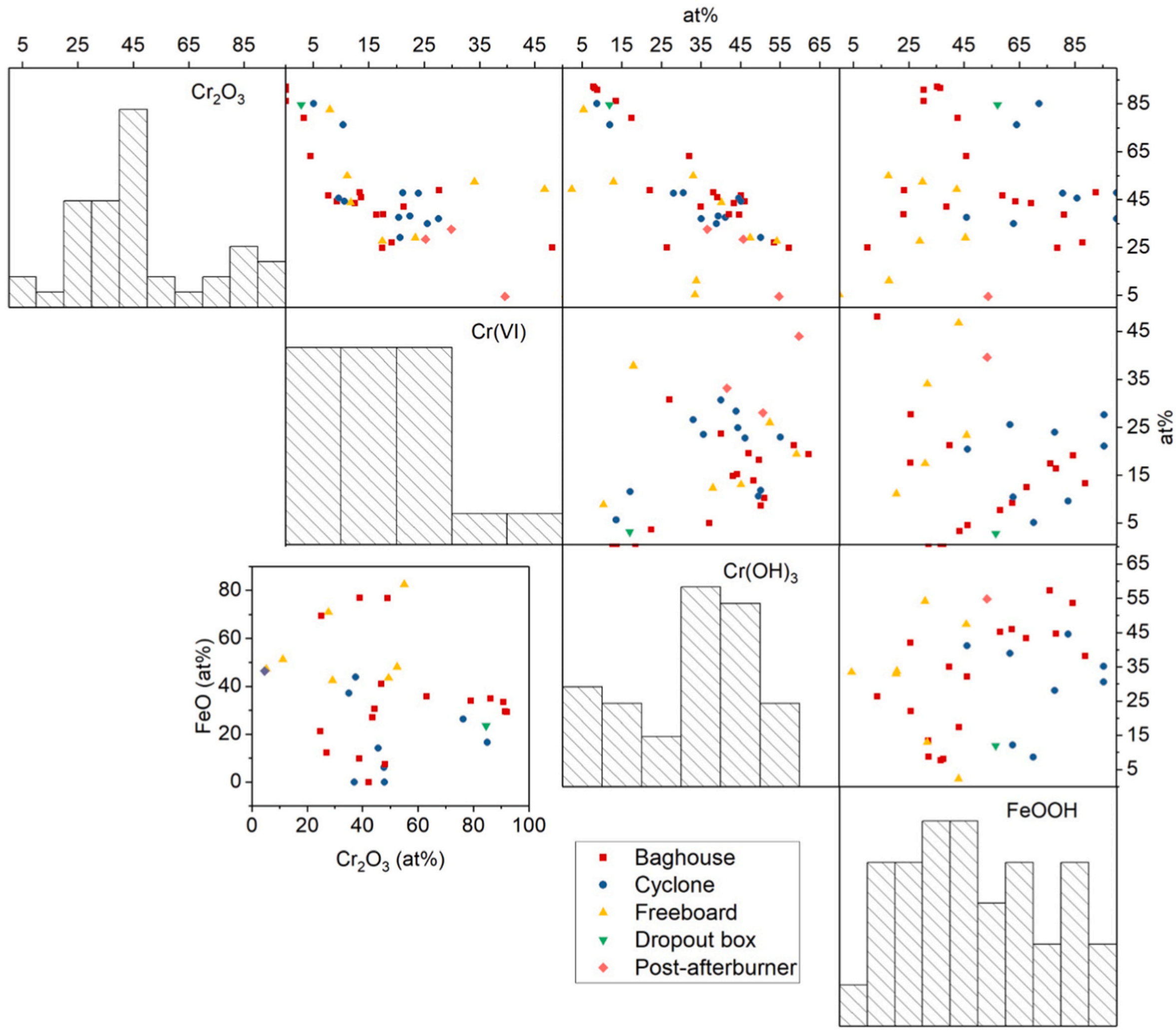

Fig. 6. Fe and Cr surface speciation of individual dust samples collected from the freeboard, dropout box, post-afterburner, cyclone, and baghouse across all tests.

The intensity of the pre-edge peak was used by Zachara et al. (2004) to quantify the proportion of Cr(VI) in contaminated soil samples. Similarly, we estimated the proportion of Cr(VI) species making up the bulk Cr K-edge spectra by mixing two end members, chromite and Na_2CrO_4 spectra. Mixing results as shown in SI Fig. 6 indicate that the observed Cr K-edge spectra have pre-edge peak intensities that are between the binary mixture of 20% Na_2CrO_4 and 80% chromite, and 0% Na_2CrO_4 and 100% chromite. These chromate concentrations reaching 20% of bulk Cr are lower than those determined on particle surfaces (Table 3; SI Table 4).

3.4.2. *Fe speciation*

The Fe K-edge XANES spectra of the ferrochrome-smelter dusts show notable variability between different sampling locations. The spectra for all dusts collected from the furnace freeboard share the edge and pre-edge features found in the Fe K-edge spectrum of chromite (Fig. 7). In contrast, dusts collected from sampling locations along the off-gas handling stream (i.e., post-afterburner, cyclone, and baghouse) have Fe K-edge spectra more similar to that of the goethite standard (Fig. 7; SI Fig. 7). The relative proportion of the different Fe standards needed to reconstruct the Fe K-edge XANES spectra of each of the dust samples was constrained by LCA. Various combinations of chromite, magnetite, hematite, goethite and ferrihydrite standards including those measured during earlier experiments (Paktunc et al., 2013; Paktunc 2015) were tested in the fittings. Maghemite and magnetite spectra show broad similarities with the exception of the white line positions (Okudera et al., 2012; Girod et al., 2015). Because the E0 values were allowed to vary during fitting, magnetite values listed in SI Table 5 should be considered as representing both magnetite and maghemite. This fitting strategy is justified because the intent of the linear combination fitting is to determine the changes in the relative proportions of the Fe(II) and Fe (III) species between the freeboard and off-gas stream dusts. The fitting results indicate that chromite along with magnetite/maghemite are the predominant species in the Fe K-edge spectra of the freeboard dusts, with lesser contributions from goethite and hematite. In contrast, the Fe (III) species, goethite and hematite dominate dusts from the off-gas handling stream, with lesser contributions from chromite (Fig. 8; SI Fig. 7; SI Table 5). Freeboard dusts have an average $Fe^{3+}/\Sigma Fe$ ratio of 0.44 ± 0.16 whereas it is 0.74 ± 0.15 for the off-gas dusts including the post after-burner, cyclone and baghouse dusts. These are conservative numbers with the assumption that magnetite/maghemite have 0.33 mol Fe^{2+} instead of 0 as in maghemite. Chromite is dominated by Fe^{2+} ($Fe^{3+}/\Sigma Fe = 0.14$) as per the average composition of chromite for the Ring of Fire deposits. The dropout box has an average $Fe^{3+}/\Sigma Fe$ ratio of 0.5.

4. Discussion

There are important distinctions between the dust-sampling locations that need to be considered when interpreting the compositional

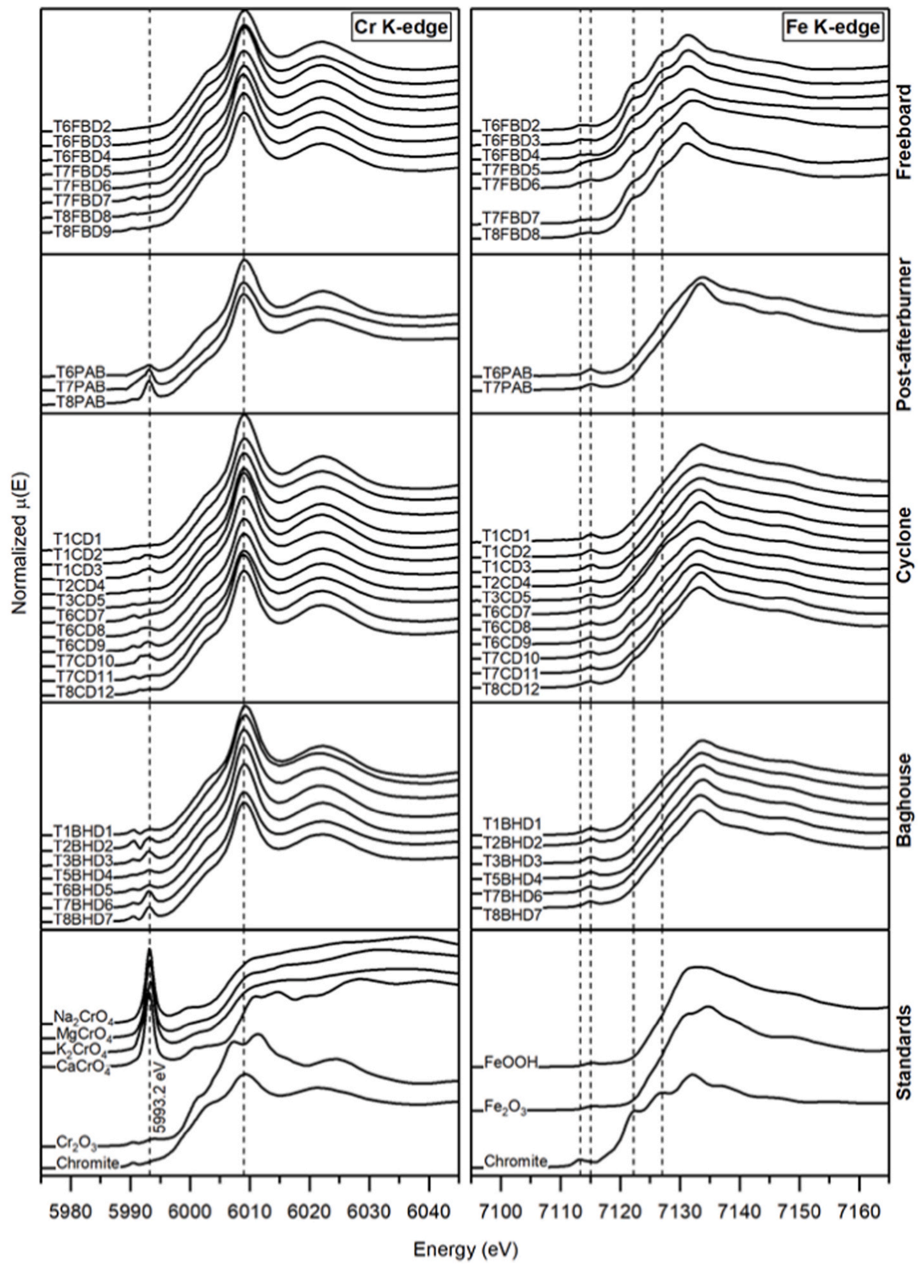

Fig. 7. XANES spectra around the Cr and Fe K-edges for dust samples collected from the freeboard, post-afterburner, cyclone, and baghouse. Spectra of relevant standards are shown for comparison and key features identified in the standards and the sample spectra are highlighted by dashed lines.

and speciation data. Dusts from the furnace freeboard were passively sampled on filters, indiscriminate of dust particle size. In contrast, dusts along the off-gas stream were primarily collected using dust separators that target certain size fractions of dust. For instance, the dropout box and the cyclone are inertial dust separators that remove coarser and finer size fractions of dust, respectively (Fig. 1). At the end of the off-gas handling system, the baghouse contains filters that separate the finest dusts from the off-gas (particle-size distribution data available in SI Fig. 8). Owing to these differences, the freeboard dusts contain a wide range of dust particle sizes, as shown by their microscopic characterization (Berryman et al., 2020; Berryman and Paktunc 2021). In contrast, the cyclone and baghouse dusts comprise more restricted size fractions of intermediate and very fine dust particles, respectively (Berryman et al., 2020). Previous micro-characterization of the dusts revealed that they comprise a mixture of feed material, glassy spherules, and slag, with the spherules being increasingly abundant in dusts collected further down the off-gas handling stream and that the higher abundance of spherules captured in the cyclone and baghouse reflects the fine particle size of the spherules, with some as small as 100 nm being identified (Berryman and Paktunc 2021; SI Fig. 8).

4.1. Ferrochrome DC-smelter dust compositions along the off-gas stream

The differences between the composition of dusts generated during ferrochrome smelting and the feed composition reflects the relative proportion of feed-material dust particles, including lime derivative of the limestone flux, slag, and spherules in the dusts captured at different points in the smelter. The glassy spherules are highly heterogeneous in composition, but predominantly $MgO–SiO_2$ rich, with variable amounts of dissolved Cr, Al, Fe, and Ca (Berryman and Paktunc 2021). Agglomerations of <1-μm Si-rich spherules similar to those described here have also been described in baghouse dusts collected from industrial ferrochrome smelters (Beukes et al., 1999; Huvinen 2001). These earlier observations are consistent with the bulk compositions of the dusts

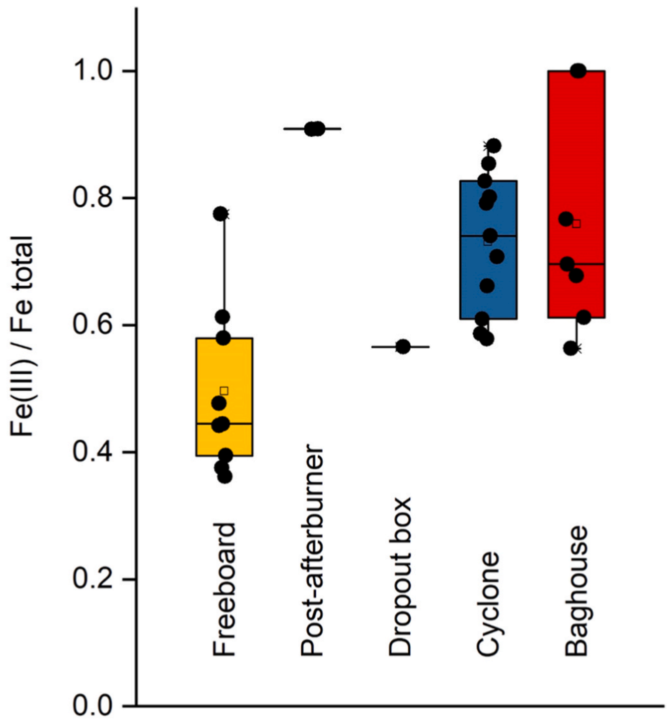

Fig. 8. Proportion of Fe(III) out of total Fe (i.e., Fe(II) + Fe(III)) based on linear combination fitting of the Fe XANES spectra (SI Table 5). Data points indicate values for individual samples from the respective sampling locations. Box-and-whisker plots indicate the 25, 50, and 75th percentile ranges. The open square symbol indicates the mean of the data.

measured here. The enrichment of the cyclone and baghouse dusts in SiO_2 and MgO relative to the feed reflects the high abundance of spherules in dusts sampled from these locations (Fig. 4). The generally closer agreement between the composition of dusts sampled from the furnace freeboard and the feed in turn reflects the higher proportion of feed materials present in freeboard dusts. The exception to this tendency is the enrichment of the freeboard dusts in CaO (Fig. 4), which reflects the relatively high amount of flux present in the vapour inside the furnace.

Changes to the size fraction of the ore in the feed or the ore feed-rate had no observable effect on the bulk composition of the dusts relative to the feed composition. This is shown by the relatively consistent compositional behavior of the dusts relative to the feed composition as a function of test conditions (SI Figs. 1 and 2). Instead, the composition of the dusts depends primarily on the sampling location and potentially the feed composition. Variation in the feed composition in our smelter tests was limited and may not have been sufficient to influence dust compositions (Fig. 3).

Comparison of the bulk dust compositions to the respective compositions of the feed, ore, and slag provides further insight into the relative abundance of these components in the dusts (Fig. 3). The ratio of Cr_2O_3 to Fe_2O_3(total) in dusts sampled from the cyclone and the freeboard is consistent with their ratio in the ore/feed, as indicated by the straight line in the associated panel in Fig. 3. Chromite is the primary Cr and Fe host in the ore and feed. This compositional trend therefore reflects the control that chromite abundance exerts on the relative proportion of Fe and Cr in the cyclone and freeboard dusts. The baghouse dusts are distinguished from the other dusts by a general enrichment in Fe relative to the ore and the freeboard and cyclone dusts (Fig. 3). The slags are expected to be deficient in Fe relative to Cr because FeO and Fe_2O_3 reduce at much lower temperatures than Cr_2O_3 as per Ellingham diagrams (Ellingham 1944) and empirical evidence (Rankin 1979). Aerosolized slag would therefore not be expected to increase the Fe content of the baghouse dusts. It is therefore likely that the higher Fe content of these fine dusts reflects an increased abundance of spherules.

Unlike in the case of Fe and Cr, the Al content of the dusts diverges significantly from that of the ore. The majority of the dusts sampled in all locations of the furnace are enriched in Al relative to the Cr_2O_3–Al_2O_3 ratio of the ore/feed (Fig. 3). The $Fe_2O_{3(total)}$-Al_2O_3 ratios of the dusts are variable, but scatter around the $Fe_2O_{3(total)}$-Al_2O_3 ratio of the ore/feed (Fig. 3). Comparison of the dust compositions to that of the slags in Cr_2O_3–Al_2O_3–$Fe_2O_{3(total)}$ spaces reveals that the behavior of Fe and Al can be at least partially explained by varying the abundance of aerosolized slag in the dusts. This is facilitated by the large variability in the Cr_2O_3, $Fe_2O_{3(total)}$, and Al_2O_3 contents of the slags collected during smelting, which may reflect varying degrees of contamination by ferrochrome (i.e. small molten alloy blebs suspended in oxide melt).

The slags are generally consistent in terms of their SiO_2, MgO, and CaO contents, reflecting the targeted basic slag composition. The presence of slag in the dusts cannot explain the variability in dust compositions for these constituents (Fig. 3). The SiO_2 and MgO contents of different dust samples must instead reflect the relative prevalence of the SiO_2–MgO-rich glassy spherules. This interpretation is supported by the negative correlation between SiO_2 or MgO and Cr_2O_3, $Fe_2O_{3(total)}$, and to a lesser extent Al_2O_3 in the dust compositions, especially the baghouse dusts (Fig. 3). The particularly strong negative correlation between Cr_2O_3 and SiO_2 or MgO in the baghouse dusts presents a compelling argument that these dusts largely comprise a mixture of chromite ore and the SiO_2–MgO-rich spherules (Fig. 3). This correlation is weaker in the cyclone dusts, and arguably absent in the freeboard dusts, which is consistent with the spherules representing a smaller component of these dusts. These interpretations are further reinforced by correlations between SiO_2 and MgO (Fig. 3); whereas the baghouse dusts and to a lesser extent the cyclone dusts show a clear positive correlation between these two constituents, the freeboard dust compositions largely plot near the feed/ore and slag compositions. The XRD results of the dust samples also support this interpretation. The predominate mineral forsterite likely occurs as quench crystals within the spherules, with chromite and periclase also identified as major crystalline phases (SI Table 3).

The freeboard dusts are distinctly enriched in CaO relative to the other dusts, as well as relative to the feed, as discussed above. Fig. 3 shows that the freeboard dusts are also enriched in CaO relative to the slags. As stated above, this reflects the presence of significant amounts of limestone flux, or its derivatives, in the freeboard dust. This is similar to an observation noted by Omran and Fabritius (2017) in electric arc furnace and ferrochrome converter dusts. Bulk compositional (Fig. 3) and XRD data (SI Table 3) also show that a number of the cyclone samples contain significant amounts of the lime component. In contrast, the baghouse dusts have a lower, broadly consistent, CaO content, reflecting the low abundance of lime, or feed materials in general, in these dusts.

The distinction of the slag and the SiO_2–MgO-rich spherules as components in the dusts based on the bulk compositional data provides additional insight into the origin of the spherules. Whereas the slag component represents aerosolized melt entrained in the furnace off-gas, the glassy SiO_2–MgO-rich spherules likely represent quenched off-gas condensates (Berryman and Paktunc 2021). This interpretation has been suggested previously (Maine et al., 2005; Huvinen 2001) and is consistent with our findings here.

Considered together, the bulk compositions of the dusts from different parts of the smelter indicate that primary dust-forming components vary between the furnace and down the off-gas handling stream. Dusts found in the vapour overlying the smelter open-bath comprise an amount of flux that exceeds the proportion found in the feed, as well as ore, and lesser amounts of aerosolized slag and gas condensates (SiO_2–MgO-rich spherules). Bulk freeboard dust compositions plot in the $Ca_2MgSi_2O_7$, $Ca_2MgSi_2O_7$, forsterite, and monoxide (MgO and CaO) fields of the SiO_2–CaO–MgO phase diagram (SI Fig. 9). Individual spherule compositions as determined by electron microprobe (Berryman and Paktunc 2021) plot largely in the monoxide (MgO and CaO) and forsterite fields (SI Fig. 9). The spherules are quenched aerosolized melt droplets that form within the furnace at extremely high temperatures in excess of 1700 and reaching 2600 °C (SI Fig. 9). Forsterite and periclase, as identified by powder-XRD, likely occur as quench crystals within the spherules. As the furnace off-gas travels down the off-gas handling stream, it passes through the different dust separators (dropout box, cyclone, and baghouse), each of which is designed to capture an increasingly finer fraction of dust. Correspondingly, the amount of feed (ore or flux) in the dust is reduced along the off-gas stream, representing a lesser component in the cyclone dust and a minor component of the baghouse dust. Instead, due to their fine grain-size, the proportion of SiO_2–MgO-rich spherules, or high-temperature condensates, increases along the off-gas handling stream, becoming a major component of the baghouse dusts. A proportion of the fine dust components, including the spherules, are captured by the coarse-dust separators as agglomerations or when they are found coating coarser dust grains (Berryman et al., 2020).

4.2. Cr and Fe oxidation in the ferrochrome smelter system

The bulk XPS and XANES results indicate that DC-furnace ferrochrome-smelter dusts contain Cr and Fe in a mixture of valence states [Cr(0), Cr(III), and Cr(VI); Fe(0), Fe(II) and Fe(III)]. These findings are consistent with earlier μXANES characterization of the dusts, which showed that a single dust sample can contain all three oxidation states of Cr, along with possible intermediate species (Berryman and Paktunc 2021). Importantly, Cr(VI) in the dusts has been shown to be hosted by the Si–Mg-rich spherules within both the freeboard dusts (sampled prior to passing through the after-burner), and dusts from down the off-gas handling stream (sampled after passing through the after-burner).

4.2.1. Cr and Fe oxidation in the furnace

Although Cr(VI) was previously identified in the freeboard dust samples using μXANES (Berryman and Paktunc 2021), its overall abundance in dusts collected from within the furnace freeboard is too low to be detected by bulk XANES (i.e. lower than about 5% of total Cr). The majority of Cr in the freeboard dusts occurs as Cr(III) hosted by chromite (Fig. 7). This is consistent with the overall abundance of chromite particles entrained in the freeboard dust, as indicated by chromite's control on the Cr_2O_3 to Fe_2O_3(total) ratio in the dusts (Fig. 3). Despite low bulk abundance, Cr(VI) is sufficiently abundant on the freeboard-dust surfaces to be detected by XPS. Indeed, the highest proportion of surficial Cr occurring as Cr(VI) was detected on freeboard dust (Fig. 5; Table 3).

The behavior of Fe in the freeboard dusts is generally comparable to the behavior of Cr. Despite also being predominantly hosted by chromite (see discussion above), Fe experiences some oxidation and hydration within the freeboard. Between 17.6 and 45.4 at% of surficial Fe (Table 3) and between 4.5 and 32.5 at% of Fe in the bulk freeboard dusts (SI Table 5) occur as Fe(III) species in goethite (FeOOH) and hematite (Fe_2O_3). The higher proportion of Cr(VI) and Fe(III) as FeOOH and Fe_2O_3 occurring on dust surfaces compared to the bulk dusts suggests that the oxidation of Cr and Fe may primarily be a surface feature in the freeboard dusts. However, caution must be taken in comparing the surface vs bulk speciation data in these samples, as the freeboard dusts comprise a wide range of particle sizes (nm to hundreds of μm) (Berryman et al., 2020). In scanning electron microscopy photomicrographs of the dust samples, fine dust particles, including abundant glassy spherules, commonly electrostatically coated coarser dust particles in the freeboard dusts. Whereas the coarser particles, dominated by feed materials in the freeboard, dominate the bulk signal, it is unclear to what extent fine particles, especially any nanoparticles, affect the surface speciation results. It is therefore also possible that the higher Cr(VI) and Fe(III) (FeOOH and Fe_2O_3) values on the freeboard dust surfaces represent contributions from the fine dust particles that electrostatically coat the coarser grains.

The identification of Cr(VI), $Cr(OH)_3$, and FeOOH within the freeboard dusts (Fig. 5) reveals that despite the overall reducing conditions in the furnace freeboard (Fig. 2), Cr and Fe oxidation (and hydration) is able to occur in the high-temperature vapour. The strong negative correlation between Cr(VI) and Cr_2O_3 further suggests that Cr(VI) formation is primarily occurring by oxidation of Cr(III) from Cr_2O_3, instead of $Cr(OH)_3$ (Fig. 6).

4.2.2. Cr and Fe oxidation in the off-gas handling stream

In addition to comprising an increasing proportion of spherules, dusts separated along the off-gas handling stream are also distinctly more oxidized and hydrated. Fe within the cyclone and baghouse dusts is no longer dominated by Fe(II) hosted by chromite, but instead has distinctly higher Fe(III) contents, occurring as FeOOH and Fe_2O_3, in both the bulk dusts (Figs. 7 and 8) as well as on the dust surfaces (Fig. 5). On average, 42 ± 20 at% of bulk Fe (SI Table 5) and between 64 and 100 at% of surficial Fe (Table 3) in the cyclone dust occurs as goethite (FeOOH) and hematite (Fe_2O_3). In the baghouse dust, 29.6 ± 15.6 at% of bulk Fe (SI Table 5) and between 30.4 and 92.7 at% of surficial Fe (Table 3) occurs as FeOOH. In addition, up to 36.3 at% of surface Fe species occur as Fe_2O_3 (Table 3; SI Table 4), some of which may be representative of maghemite (SI Table 3) and/or hematite (SI Table 5). The close agreement between the surficial and bulk behavior of Fe likely reflects the much smaller average particle size of the baghouse dusts (<2 um) and the higher proportion of spherules. This is also consistent with chromite not exerting a full control on Fe concentrations in the baghouse dusts, as indicated by the Cr/Fe ratio in the baghouse dusts being lower than in the chromite ore (Fig. 3).

Unlike in the freeboard dusts where only surficial Cr(VI) was detected, Cr(VI) concentrations are sufficiently high in dusts separated from the off-gas to be detected in the bulk dusts (Fig. 7). The highest bulk Cr(VI) signals correspond to samples from the post-afterburner and the baghouse. Although the spherules contain generally low concentrations of Cr (see discussion above), they are the primary hosts of Cr(VI) (Berryman and Paktunc 2021). As a result, regardless of the abundance of chromite in the baghouse dusts, chromite remains the primary Cr-hosting phase (Fig. 7). The high abundance of spherules in the baghouse results in the presence of sufficient Cr(VI) to be detected via the presence of the pre-edge peak at 5993.2 eV (Fig. 7). Moreover, the abundance of Cr(VI) is strongly correlated to FeOOH in the surfaces of the baghouse dusts (Fig. 6), further underlining the oxidized and hydrated nature of both Fe and Cr in the spherules.

4.3. Implications for ferrochrome smelting in a DC arc furnace

The results indicate that Cr(VI) occurs in dusts within the DC furnace freeboard off gas, demonstrating that Cr(III) oxidation can occur in a DC furnace's freeboard. It has generally been assumed that closed ferrochrome furnaces (i.e. DC furnaces as considered in this paper, but also some SAFs), wherein oxygen availability is limited in the freeboard, generate less or no Cr(VI) compared to open/semi-open SAFs (Beukes et al., 2017). This assumption is founded on the ideal thermodynamic behavior of the system, where no oxygen is accessible to the furnace off-gas and only Cr reduction occurs. In reality, oxygen ingress into closed furnaces is possible because the pressure in the furnace is usually slightly lower than outside the furnace to prevent CO combustion taking place on the furnace roof (outside the furnace). The presence of high amounts of CaO in the furnace vapour has also been linked to Cr(VI) formation in a closed furnace (Berryman and Paktunc, 2021). Accordingly, as the results presented here reveal, high temperatures in the furnace combined with volatile species (Jones et al., 2011) and a small amount of oxygen can produce Cr(VI) in the freeboard dusts. The open bath nature of the DC furnaces exposes the feed material in the freeboard, including fine chromite dust and the Ca-rich flux, to the high temperatures above the bath and in proximity to the arc. This is unlike closed SAFs where the freeboard is insulated from the molten slag below by the burden and the arc is not exposed, such that freeboard dust is subjected to much lower temperatures.

Chromite is the only source of Cr and Fe in ferrochrome smelter dusts. A processing advantage of DC furnaces is their ability to accommodate chromite fines in the feed and without the need of pelletization (Jones et al., 2011; Jones and Erwee 2016). However, this advantage may result in more chromite in the high temperature off-gasses above the smelter bath. Our results identified significant concentrations of Cr (VI) occurring on dust particle surfaces, concentrations that exceed the bulk Cr(VI) abundance. It is therefore possible that the high reactive surface areas of the fine chromite particles exposed to high temperatures and volatiles above the open bath have the potential to generate dust with Cr(VI). As a result, fine chromite-containing materials, including recycled dust, could potentially be partially oxidized in the freeboard, leading to increasingly higher Cr(VI) concentrations in the freeboard dust. To reduce the amount of dust generated during smelting, possible preventative measures that could be explored include micro-pelletization of fine chromite and charge materials before they are fed to the furnace. In addition, in current applications, reductant particles in the freeboard of DC furnace do not prevent exposure of chromite particles to oxidizing fumes, because the reductant and chromite particles are not in physical contact. To remedy this, another approach to consider may include mixing small amounts of reductant with fine chromite during micro-pelletization, similar to the pellet design used in the Premus technology (Naiker 2007) or the new direct reduction of chromite process where chromite is in physical contact with reductant particles (Paktunc et al., 2018; Yu and Paktunc 2018). This approach may create a sufficiently reducing local environment around the fine chromite particles in the pellets to prevent their oxidation. Any approach to reduce dust generation or Cr(VI) formation in DC furnaces would need to be tested for efficacy.

The design of the pilot DC furnace smelter used in this study includes an after-burner to combust the CO-bearing off-gases. However, after-burners are not commonly used in the ferrochrome industry in conjunction with DC furnaces. The off-gas from most commercial DC furnace are cleaned with wet venturi systems, with the resulting cleaned CO-rich off gas being used as an energy source or flared. It has been previously shown that the flaring of the off-gas could result in additional Cr(VI) formation (Du Preez et al., 2015). The capture of dusts before and after the after-burner in this study reveals that the after-burner is not solely responsible for the oxidation of Cr and the formation of Cr(VI). As a result, the use of a DC furnace without an after-burner does not absolve a ferrochrome producer from proper off-gas dust capturing and treatment.

As reported by Berryman and Paktunc (2021), the high Cr(VI) content of off-gas dust is a function of the high proportion of spherules. This is consistent with the observations of Gericke (1995) in that Cr(VI) occurs within the off-gas condensates (spherules) and not just on oxidized dust particle surfaces. Spherules are generally very fine in size, reaching the nanoparticle size range (Berryman et al., 2020). For instance, Cox et al. (1987) found that 55% of the total Cr(VI) in baghouse dusts was associated with particles that are less than 0.7 μm in size, accounting for 12% of the dust mass. This raises the question of the effectiveness of conventional dust-capture and filter systems in capturing the ultrafine Cr(VI)-bearing fraction, as well as the efficacy of leaching of Cr(VI) from within the glassy spherules. Wet scrubbers struggle to separate particles smaller than 1 μm (Beukes et al., 2017); therefore, additional sintered plate filtering of the post wet scrubber un-combusted off gas may be needed to achieve residual particle levels of approximately 1 $mg.Nm^3$ (Niemela et al., 2004). However, our understanding is that ceramic filters may also have a limited ability to capture sub-micron particles. This is a research gap that remains to be addressed. Moreover, to better constrain the relative proportion of surface-bound Cr(VI) versus bulk Cr (VI) contents of the dusts, and its implications for dust treatment, our study findings motivate further investigations into the different size fractions of dust.

5. Conclusions

Dusts collected from both within the DC furnace freeboard as well as along the off-gas handling stream are dominated by chromite, forsterite, MgO, CaO, aerosolized slag and glassy spherules. Spherules interpreted as off-gas condensates become increasingly abundant in the finer fractions of dust, separated along the off-gas handling stream. Cr and Fe occur in multiple oxidation states [i.e. Cr(0), Cr(III), Cr(VI), Fe(0), Fe(II), and Fe(III)] in the form of various anhydrous [Cr_2O_3 or FeO and Fe_2O_3 in chromite or Cr(VI)] and hydrous [FeOOH and $Cr(OH)_3$] species in dusts collected from all parts of the smelter system. Cr is primarily hosted by chromite in dusts collected from the furnace as well as from dusts separated from the off-gas. FeOOH and Cr(VI) occur in higher proportion in the spherule-rich dusts collected from the off-gas handling stream, especially from the baghouse. Whereas both Fe and Cr primarily occur as Fe(II) and Cr(III) hosted by chromite in the freeboard, Fe in the off-gas stream occurs predominantly as Fe(III) in FeOOH and an increasing proportion of Cr occurs as Cr(III) in $Cr(OH)_3$. Cr(VI) occurs as surface species in all the dust samples.

Our results suggest that despite the overall reducing conditions in the furnace, the open-bath nature of the DC furnace and the presence of chromite fines in the feed are conducive for the formation of Cr(VI) within the furnace freeboard. Cr(VI) forms in the furnace when the fine dust particles are exposed to the high temperatures in the off-gas. Smelting approaches that reduce dust generation in DC furnaces, especially the presence of chromite fines and flux in the off-gas dusts, such as micro-pelletization, could possibly reduce Cr(VI) formation. However, this approach remains to be tested.

In addition to preventative measures, current dust-capture and treatment techniques need to be optimized for the finest fraction of dust, which hosts the majority of Cr(VI). This includes an assessment of the effectiveness of conventional dust-capture and filter systems, such as wet scrubbers and ceramic filters in capturing the Cr(VI)-bearing fraction in the dust, as well as better constraints on the particle size distribution of dusts and their characteristics.

Declaration of competing interest

The authors declare that they have no known competing financial interests or personal relationships that could have appeared to influence the work reported in this paper.

Acknowledgements

Pilot-scale smelter tests were carried out by Glencore's Expert Process Solutions group in Sudbury. Jeffrey Scott and Derek Smith helped with sample preparation and characterization work at CanmetMINING. This research utilized resources of Beamline for Materials Measurement (6-BM) of the National Synchrotron Light Source II, a U.S. Department of Energy (DOE) Office of Science User Facility operated for the DOE Office of Science by Brookhaven National Laboratory under Contract No. DE-SC0012704. Bruce Ravel performed the XANES experiments at NSLS-II. The study was funded by Natural Resources Canada, Government of Canada, under the Rare Earth Elements and Chromite R&D Initiative.

Appendix A. Supplementary data

Supplementary data to this article can be found online at https://doi.org/10.1016/j.clet.2021.100386.

References

Arcon, I., Mirtic, B., Kodre, A., 1998. Determination of valence states of chromium in calcium chromates by using X-ray absorption near-edge structure (XANES) spectroscopy. J. Am. Ceram. Soc. 81, 222–224.

Arita, A., Costa, M., 2011. Environmental agents and epigenetics. In: Handbook of Epigenetics. New York University School of Medicine, NY, pp. 459–476.

Ashley, K., Howe, A.M., Demange, M., Nygren, O., 2003. Sampling and analysis considerations for the determination of hexavalent chromium in workplace air. J. Environ. Monit. 5, 707–716.

Bartlett, R.J., James, B.R., 1988. In: Nriagu, J.O., Nieboer, E. (Eds.), Chromium in the Natural and Human Environments. Wiley, New York.

Berryman, E.J., Paktunc, D., 2021. Cr(VI) formation in ferrochrome-smelter dusts. J. Hazard Mater. (accepted).

Berryman, E.J., Paktunc, D., Goodall, G., 2020. Generation and capture of ferrochrome smelter dusts from a pilot-scale DC electric-arc furnace. In: Proceedings of the 59th Conference of Metallurgists, COM 2020. The Canadian Institute of Mining, Metallurgy and Petroleum.

Beukes, J.P., du Preez, S.P., van Zyl, P.G., Paktunc, D., Fabritius, T., Päätalo, M., Cramer, M., 2017. Review of Cr(VI) environmental practices in the chromite mining and smelting industry - relevance to development of the Ring of Fire, Canada. J. Clean. Prod. 165, 874–889.

Beukes, J.P., Pienaar, J.J., Lachmann, G., Giesekke, E.W., 1999. The reduction of hexavalent chromium by sulphite in wastewater. WaterSA 25, 363–370.

Bianconi, A., Garcia, J., Benfatto, M., Marcelli, A., Natoli, C.R., Ruiz-Lopez, M.F., 1991. Multielectron excitations in the K-edge x-ray-absorption near-edge spectra of V, Cr, and Mn 3d0 compounds with tetrahedral coordination. Phys. Rev. B 43, 6885.

Biesinger, M.C., Payne, B.P., Grosvenor, A.P., Lau, L.W.M., Gerson, A.R., Smart, R.S.J., 2011. Resolving surface chemical states in XPS analysis of first row transition metals, oxides and hydroxides: Cr, Mn, Fe, Co and Ni. Appl. Surf. Sci. 257, 2717–2730.

Biesinger, M.C., Brown, C., Mycroft, J.R., Davidson, R.D., McIntyre, N.S., 2004. X-ray photoelectron spectroscopy studies of chromium compounds. Surf. Interface Anal. 36, 1550–1563.

Calvin, S., 2013. XAFS for Everyone. CRC Press, Boca Raton, FL.

Cox, X.B.I., Linton, R.W., Butler, F.E., 1985. Determination of chromium speciation in environmental particles. Multitechnique study of ferrochrome smelter dust. Environ. Sci. Technol. 19, 345–352.

Du Preez, S.P., Beukes, J.P., van Dalen, W.P.J., van Zyl, P.J., Paktunc, D., Loock-Hattingh, M.M., 2017. Aqueous solubility of Cr(VI) compounds in ferrochrome bag filter dust and the implications thereof. WaterSA 43, 298–309.

Du Preez, S.P., Beukes, J.P., Van Zyl, P.G., 2015. Cr (VI) generation during flaring of CO-rich off-gas from closed ferrochromium submerged arc furnaces. Metall. Mater. Trans. B 46, 1002–1010. https://doi.org/10.1007/s11663-014-0244-3.

Ellingham, H.J.T., 1944. Reducibility of oxides and sulphides in metallurgical processes. J. Soc. Chem. Ind., London 63, 125. https://doi.org/10.1002/jctb.5000630501.

Gericke, W., 1995. Environmental aspects of ferrochrome production. In: Proceedings of 7th International Ferroalloys Congress. Trondheim, Norway.

Girod, M., Vogel, S., Szczerba, W., Thunemann, A.F., 2015. How temperature determines formation of maghemite nanoparticles. J. Magn. Magn Mater. 380, 163–167.

Grosvenor, A.P., Kobe, B.A., Biesinger, M.C., McIntyre, N.S., 2004. Investigation of multiplet splitting of Fe 2p XPS spectra and bonding in iron compounds. Surf. Interface Anal. 36, 1564–1574.

Haggerty, S.E., 1991. Oxide mineralogy of the upper mantle. In: Lindsley, D.H. (Ed.), Oxide Minerals: Petrologic and Magnetic Significance. Reviews in Mineralogy, 25. Mineralogical Society of America, pp. 355–416.

Huvinen, M., 2001. Surface structure and speciation of metal aerosols: a key to the understanding of their biological effects. In: Ebdon, L., Pitts, L., Cornelis, R., Crews, H., Donard, O.F.X., Quevauviller, P. (Eds.), Trace Element Speciation for Environment, Food and Health. The Royal Society of Chemistry, Cambridge, pp. 308–314.

Irvine, T.N., 1965. Chromian spinel as a petrogenetic indicator. Part 1. Theory. Can. J. Earth Sci. 2, 648–672.

Jones, R.T., 2014. DC arc furnaces - past, present, and future. In: Mackey, P.J., Grimsey, E.J., Jones, R.T., Brooks, G.A. (Eds.), Celebrating the Megascale. Springer, Cham. https://doi.org/10.1007/978-3-319-48234-7_10.

Jones, R.T., Erwee, M.W., 2016. Simulation of ferro-alloy smelting in DC arc furnaces using Pyrosim and FactSage. Calphad Comput. Coupling Phase Diagrams Thermochem. 55, 20–25.

Jones, R.T., Reynolds, Q.G., Curr, T.R., Sager, D., 2011. Some myths about DC arc furnaces. J. S. Afr. Inst. Min. Metall 111, 665–673.

Ma, G., Gerbers-Craig, A.M., 2006. A review on the characteristics, formation mechanism and treatment processes of Cr(VI)-containing pyrometallurgical wastes. J. S. Afr. Inst. Min. Metall 106, 753–763.

Maine, C.F., Smit, J.P., Giesekke, E.W., 2005. The Solid Stabilization of Soluble Wastes Generated in the South African Ferrochrome Industry. Water Research Commission, South Africa.

Naiker, O., 2007. The development and advantages of Xstrata's Premus Process. In: Proceedings Ferroalloys 11th International Congress, pp. 112–119.

Niemela, P., Krogerus, H., Oikarinen, P., 2004. Formation, characterization and utilization of CO-gas formed in ferrochrome smelting. In: Proceedings of 10th International Ferroalloys Congress, pp. 68–77. Cape Town, South Africa.

Okudera, H., Yoshiasa, A., Murai, K., Okube, M., Takeda, T., Kikkawa, S., 2012. Local structure of magnetite and maghemite and chemical shift in Fe K-edge XANES. J. Mineral. Petrol. Sci. 107, 127–132.

Omran, M., Fabritius, T., 2017. Effect of steelmaking dust characteristics on suitable recycling process determining: ferrochrome converter (CRC) and electric arc furnace (EAF) dusts. Powder Technol. 308, 47–60.

Oze, C., Bird, D.K., Fendorf, S., 2007. Genesis of hexavalent chromium from natural sources in soil and groundwater. Proc. Natl. Acad. Sci. Unit. States Am. 104, 6544–6549.

Paktunc, D., 2016. Phase transformations in the system Fe-AsO4-SO4 and the structure of amorphous ferric arsenate: implications for arsenic stabilization in mine drainage and industrial effluents. Can. Mineral. 53, 921–936. https://doi.org/10.3749/canmin.1500040.

Paktunc, D., Thibault, Y., Sokhanvaran, S., Yu, D., 2018. Influences of alkali fluxes on direct reduction of chromite for ferrochrome production. J. S. Afr. Inst. Min. Metall 118, 1305–1314.

Paktunc, D., Manceau, A., Dutrizac, J., 2013. Incorporation of Ge in ferrihydrite: implications for the structure of ferrihydrite. Am. Mineral. 98, 848–858. https://doi.org/10.2138/am.2013.4312.

Rankin, W.J., 1979. Reduction of chromite by graphite and carbon monoxide. Trans. Ins. Mining Metall. Section C 88, C107–C113.

Ravel, B., Newville, M., 2005. ATHENA, Artemis, HEPHAESTUS: data analysis for X-ray absorption spectroscopy using IFEFFIT. J. Synchrotron Radiat. 12, 537–541.

Yu, D., Paktunc, D., 2018. Direct production of ferrochrome by segregation reduction of chromite in the presence of calcium chloride. Metals 8, 69. https://doi.org/10.3390/met8010069.

Zachara, J.M., Ainsworth, C.C., Brown, G.E., Catalano, J.G., McKinley, J.P., Qafoku, O., Smith, S.C., Szecsody, J.E., Traina, S.J., Warner, J.A., 2004. Chromium speciation and mobility in a high level nuclear waste vadose zone plume. Geochem. Cosmochim. Acta 68, 13–30.